Volume 1 | Number 1 | Jan 2013 | Pages 1–100

PCCP

Physical Chemistry Chemical Physics
www.rsc.org/pccp

ROYAL SOCIETY OF CHEMISTRY

ROYAL SOCIETY OF CHEMISTRY

www.rsc.org/pccp

ARTICLE TYPE

Core electron excitations in U^{4+}: modelling of the $nd^{10}5f^2 \rightarrow nd^9 5f^3$ transitions with n = 3, 4 and 5 by ligand field tools and density functional theory†

Harry Ramanantoanina,*[a] Goutam Kuri,*[a] Claude Daul[b] and Johannes Bertsch[a]

Ligand field density functional theory (LFDFT) calculations have been used to model the uranium $M_{4,5}$, $N_{4,5}$ and $O_{4,5}$-edges X-ray absorption near edge structure (XANES) in UO_2, characterized by the promotion of one electron from the core and the semi-core 3d, 4d and 5d orbitals of U^{4+} to the valence 5f. The model describes the procedure to resolve non-empirically the multiplet energy levels
10 originating from the two-open-shell system with d and f electrons and to calculate the oscillator strengths corresponding to the dipole allowed $d^{10}f^2 \rightarrow d^9f^3$ transitions proper to represent the d electron excitation process. In the first step, the energy and UO_2 unit-cell volume corresponding to the minimum structures are determined using the Hubbard model (DFT+U) approach. The model of the optical properties due to the uranium $nd^{10}5f^2 \rightarrow nd^9 5f^3$ transitions, with n = 3, 4 and 5, has been tackled by means of electronic structure calculations based on ligand field concept emulating the Slater-Condon integrals, the spin-orbit coupling constants and the parameters of
15 the ligand field potential needed by the ligand field Hamiltonian from Density Functional Theory. A deep-rooted theoretical procedure using LFDFT approach has been established for actinide-bearing systems that can be valuable to compute targeted results, such as spectroscopic details at the electronic scale. As a case study, uranium dioxide has been considered because it is a nuclear fuel material, and both atomic as well as electronic structures calculations are indispensable for a deeper understanding of irradiation driven microstructural changes occurring in this material.

20

Introduction

A great deal of research on actinide compounds has been carried out, with both fundamental understanding and possible applications in sight. [1-5] Actinide isotopes (such as Th, U and
25 Pu) are radioactive with a wide range of nuclear properties. Their physical as well as chemical properties are often investigated because of their industrial use in the process of generating electric energy from nuclear power plants and the safe disposal of the spent nuclear fuel. The interest in actinide compounds is also a
30 matter of tremendous investigations using computational modelling and simulations that help to overcome the experimental challenges in handling radioactive material, and to contribute to the fundamental understanding of structural and coordination chemistry of actinide compounds.
35 Understanding of the crystal chemistry and properties of actinide compounds requires a detailed insight into the final electronic distributions and character of the 5f electrons in the ground or excited configurations of the free actinide atoms. The structural, spectroscopic and electronic properties of actinide compounds
40 have been widely studied both theoretically and experimentally. [6-10] Obviously, derivation of energy levels from experimental data is often a challenging task due to multiplet electronic structure. For example the X-ray absorption and/or photoemission spectra of actinide based compounds feature multiple electron
45 correlation effects in a defined configuration. [11-12] Therefore it

is practically not simple to characterize an optical spectrum without use of a phenomenological model, which is able to illustrate the important features due to the electronic transitions.
Ligand field theory is a very successful concept for the
50 description of the bonding regime and the electronic properties of rare-earth ions in coordination chemistry. [13] It is a phenomenological model, which at the very beginning employed only empirical parameters. [14,15] Nowadays, the premise of the ligand field theory has evolved being fully implemented in
55 regular first principles quantum chemistry codes. [16-18] Although the principle of the model has not been the subject of any change, keeping its phenomenological origin, the nature of the parameters has been reformed, being derived by a purely non-empirical scheme. The ligand field Density Functional Theory
60 (LFDFT) algorithm is one of these codes, aiming reasonably to compute the multiplet electronic structure, using Density Functional Theory (DFT) based calculations. [16-18] In the last three years, the LFDFT was used to study two-open-shell electronic structures, involving at the same time f and d electrons.
65 The results, while applied to the luminescence of lanthanide compounds, were always comparable with the experimental findings. [19-22] Thus LFDFT can be considered as a valuable non-empirical tool to evaluate the electronic structure and optical properties in coordination chemistry.
70 In the following, we present LFDFT calculations of the electronic structure and the optical properties of U^{4+} in the uranium dioxide (UO_2). UO_2 is a well-described material extensively used as fuel

in nuclear industries. [23-25] Its investigation is therefore of crucial importance and comprises the bulk as well as the intrinsic defects properties for fresh (un-irradiated) materials, as well as oxidation, formation and diffusion of fission gas atoms, redistribution of fission products in the matrix of irradiated spent fuel *etc*. In this work, our results will be limited to the description of only fresh UO_2 material. We consider the core and semi-core electron excitations originating successively from the $3d$, $4d$ and $5d$ orbitals, and their mutual interaction with the strongly correlated $5f^2$ (the ground electron configuration of U^{4+}). The multiplet energy levels and the oscillator strength of the electric dipole moment of the inter-configuration $nd^{10}5f^2 \rightarrow nd^9 5f^3$ transitions, with n = 3, 4 and 5 are determined. This, in turn, allows us to calculate the X-ray absorption near edge structure (XANES) at the uranium $M_{4,5}$, $N_{4,5}$ and $O_{4,5}$ edges in UO_2.

Methodology

The phenomenological two-open-shell ligand field Hamiltonian (H), proper to describe the $nd^{10}5f^2 \rightarrow nd^9 5f^3$ transitions, with n = 3, 4 and 5, combines three independent entities: [19-21]

$$H = H_{ER} + H_{SO} + H_{LF} \tag{1}$$

where, H_{ER}, H_{SO} and H_{LF} represent the interactions due to the electron-electron repulsion, the spin-orbit coupling and the ligand field splitting, respectively.

The matrix elements of all the entities in eqn. 1 are expressed in the basis of single determinants of spin-orbitals. Therefore, the matrix elements of the electron-electron repulsion (eqn. 2) consist of the product of the Slater-Condon parameters F and G with the coefficients f and g, which depend on the angular quantum numbers of all the single determinants arising from the ground configuration $nd^{10}5f^2$ and the excited $nd^9 5f^3$.

$$H_{ER} = \sum_{k=0,2,4,6} F^k(ff)f_k(ff) + \sum_{k=0,2,4} F^k(df)f_k(df) + \sum_{k=1,3,5} G^k(df)g_k(df) \tag{2}$$

The Slater-Condon parameters representing the Coulomb F and the exchange G interactions are theoretically defined as integration over a portion of the one-electron radial functions (R) centred at the position of a U^{4+} ion (eqn. 3-5), [26,27] whereas the coefficients f and g are independent of R but particular to any actinide ions belonging to the present $nd^{10}5f^2$ and $nd^9 5f^3$ electron configurations.

$$F^k(ff) = \int_0^\infty \int_0^\infty \frac{r_<^k}{r_>^{k+1}} R_{5f}^2(r_1) R_{5f}^2(r_2) r_1^2 r_2^2 \, dr_1 dr_2 \tag{3}$$

$$F^k(df) = \int_0^\infty \int_0^\infty \frac{r_<^k}{r_>^{k+1}} R_{nd}^2(r_1) R_{5f}^2(r_2) r_1^2 r_2^2 \, dr_1 dr_2 \tag{4}$$

$$G^k(df) = \int_0^\infty \int_0^\infty \frac{r_<^k}{r_>^{k+1}} R_{nd}(r_1) R_{5f}(r_2) R_{5f}(r_1) R_{nd}(r_2) r_1^2 r_2^2 \, dr_1 dr_2 \tag{5}$$

The matrix elements of the spin-orbit coupling interaction (eqn. 6) are obtained as the product of the one-electron spin-orbit coupling constant ζ with the coefficients d, which depend on the spin and angular momentum operators defined in terms of

spherical harmonics of order $l = 3$ and $l = 2$ for the f and the d electrons, respectively.

$$H_{SO} = \zeta_{5f} d_f + \zeta_{nd} d_d \tag{6}$$

The matrix elements of the ligand field splitting are obtained from the product of the Wybourne-normalized crystal field parameters B [28] and the spherical harmonic tensor operator C acting on the f and d orbitals of U^{4+}. In total, there is a possible combination of 64 independent B parameters to compose the ligand field Hamiltonian. [26] However in case of the present cubic symmetry, there are only three parameters, which are taken into account (eqn. 7).

$$
\begin{aligned}
H_{LF} = &\; B_0^4(ff)\left[C_0^{(4)} + \sqrt{\frac{5}{14}}\left(C_4^{(4)} + C_{-4}^{(4)}\right)\right] + B_0^6(ff)\left[C_0^{(6)} - \sqrt{\frac{7}{2}}\left(C_4^{(6)} + C_{-4}^{(6)}\right)\right] \\
&+ B_0^4(dd)\left[C_0^{(4)} + \sqrt{\frac{5}{14}}\left(C_4^{(4)} + C_{-4}^{(4)}\right)\right]
\end{aligned} \tag{7}
$$

The DFT calculations have been carried out by means of the Amsterdam Density Functional (ADF) program package (ADF2014.01). [29-31] This code is a quantum chemistry code enabling the run of average of configuration (AOC) type calculation needed by the LFDFT procedure. [19-22,26,27] The AOC is a restricted DFT calculation imposing fractional occupation numbers on molecular orbitals assigned to d or f parentage. [20] The hybrid functional B3LYP has been used to compute the electronic structure and the optical properties of the cubic cluster $(UO_8)^{12-}$ embedded in UO_2. [32] A series of point charges are added in the position of the next nearest neighbour of $(UO_8)^{12-}$ in order to neutralize the high negative charge of the cluster and also to mimic the long-range interaction due to the periodicity of the UO_2 structure using a Madelung potential. The molecular orbitals were expanded using a quadruple-zeta plus polarization Slater-type orbitals (STO) functions (QZ4P) for the U atom and triple-zeta plus polarization STO functions (TZP) for the O atom. The self-consistent field (SCF) was set-up to take into account all electrons. The relativistic corrections were treated considering the Zeroth Order Regular Approximation (ZORA) of the Dirac equation as implemented in the ADF program package. [29-31] The scalar and the spin-orbit parts of the ZORA Hamiltonian were used, which provide an accurate description of both the spin-independent and spin-dependent relativistic effects inherent to heavy elements [1,33] such as uranium. [34-36]

The equilibrium structure and energies of the pristine UO_2 were theoretically determined by means of DFT based periodical calculation implemented in the Vienna Ab initio Simulation Package (VASP). [37,38] The exchange and correlation effects are described with the local density approximation (LDA) [39] and the generalized gradient approximation (GGA) functionals. [40] The following valence configurations have been considered: $6s^2 7s^2 6p^6 6d^2 5f^2$ and $2s^2 2p^4$, respectively for U and O atoms. The interaction between these valence electrons and the core ones was emulated with the projected augmented wave method. [41,42] A plane wave basis sets with a cut-off energy of 520 eV was used. 6-k points were included in each direction of the lattice according to the Monkhorst-Pack scheme. [43]

Results and Discussion

The oxidation state of the uranium ion in UO_2 is formally +4. The tetravalent uranium ion is prone to a single-open-shell electronic structure, which consists in its ground state by the population of 2 electrons in the seven-fold degenerate $5f$ orbitals. [44] Although we may believe that UO_2 has a metallic character due to this partially filled $5f$ shell, UO_2 belongs to a special class of insulating materials being a Mott-insulator. [44,45,46] Experimentally, the band gap of UO_2 is known to *circa* 2 eV [47,48] and it is predominantly characterized by the $5f^2 - 5f^2$ transitions. [49] The $5f$ orbitals of U in UO_2 interact weakly with the ligand environment (the oxygen $2p$ orbitals). [44,50-52] In this perspective, the calculated DFT band structure based on LDA or GGA functional frequently gives a metallic ground state regardless of the antiferromagnetic interaction observed in the experiments below the Neel Temperature. A realistic description of the properties is nonetheless achieved, while the computational set-up incorporates the Hubbard correction *via* the DFT+U formalism. [53,54] Recently, it has also been shown that DFT band structure algorithm operated with hybrid functional offers a good alternative to represent correctly the ground state properties of UO_2. [49,55] In this work, we realize the optimisation of the lattice parameters of UO_2 using the early concept defined in the DFT+U methodology. Based on previous theoretical studies [56-61], the Coulomb (U) and exchange (J) parameters have been set to the values of 4.5 eV and 0.5 eV, respectively. These values have been validated, which provide a realistic description of the electronic and magnetic structures of UO_2. [56-61] The definition of the U parameter itself cannot be rationalized, since U is often deduced from the experimental data. [62] On the other hand, we can justify the value of the J parameter with respect to the calculated Slater-Condon parameters that will be described later. Nevertheless, we are going to use the simplified formalism [57] by taking only the difference $U - J$ in the periodical calculation.

The crystal structure of UO_2 is graphically represented in Figure 1, where the U and O atoms are located at their ideal fluorite positions. The U atoms are eight-fold coordinated with the O atoms (Figure 1) in a cubic arrangement and these latter ones are four-fold coordinated with the U atoms in a tetrahedral symmetry.
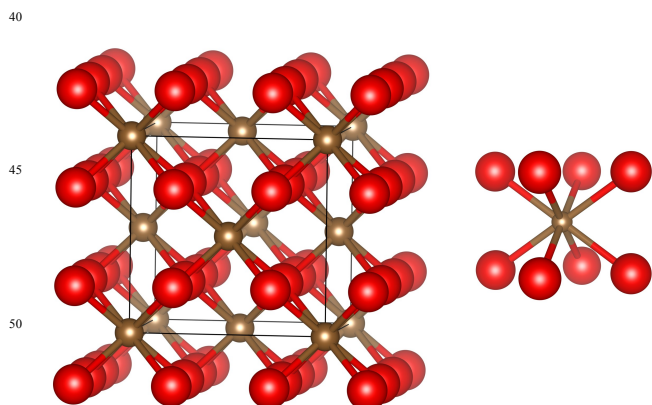
Fig. 1 Schematic representations of: the unit-cell of UO_2 (right-hand-side) crystallizing in the fluorite structure type and the cluster $(UO_8)^{12-}$ (left-hand-side) cut from the bulk structure of UO_2. Colour code: oxygen atoms are red and uranium atoms are brown.

Table 1 Optimized unit-cell volume V (in Å^3), lattice constant a (in Å), and calculated bulk modulus B (in GPa) of UO_2 obtained at the LDA+U, and GGA+U levels of theory, compared with available experimental data (Exp.); together with the calculated distances d (in Å) between U and O and two nearest U atoms.

	LDA+U	GGA+U	Exp.
V	162.23	170.94	163.73[a]
a	5.4540	5.5499	5.4707[a]
B	221.42	197.15	207[b]
d_{U-O}	2.3617	2.4032	2.3689
d_{U-U}	3.8566	3.9244	3.8684

[a] taken from ref. [63,64]; [b] taken from ref. [59]

Besides, distortion of the oxygen cage is possible due to the Jahn-Teller effect. [65,66] This is observed in neutron diffraction experiments, [67-70] but it is neglected in this work conserving the high symmetry O_h structure of the molecular cluster $(UO_8)^{12-}$ (Figure 1) embedded in UO_2. Within the fluorite structure, the lattice a, b and c constants are all equivalent and the angles α, β and γ equal 90.0°. The unit-cell volume V represents the product $a \times b \times c = a^3$. We use the traditional representation of the unit-cell of UO_2 by means of the twelve atoms in a cell, including four U and eight O atoms. [56-61] The magnetic interaction due to the valence electrons of the U atoms is approximated using the collinear $1k$ antiferromagnetic order alternating U centres along the c-axis of the unit-cell, in line with previous theoretical descriptions of UO_2. [56,59] The iterations in the self-consistent field process are therefore spin-unrestricted but the global spin-polarization is fixed to zero.

The total electronic energy is calculated with respect to the previously described conditions by varying the volume of the unit-cell. The energy and unit-cell volume corresponding to the minimum structures are determined *via* fitting of the DFT results with a second order polynomial function using the Birch-Murnaghan equation of state (see the ESI† Figure S1). [71,72]

The bulk properties of UO_2 obtained in the present DFT calculations are collected in Table 1, together with the corresponding values of experimental results reported in the literature. In general both LDA+U and GGA+U calculations yield a realistic description of the unit-cell of UO_2, since the difference in the unit-cell volume if compared to the experimental results, represents a deviation of less than 5 %. The calculated unit-cell volumes are in line with previous theoretical results based on LDA+U [73] and GGA+U [59,73] calculations. We note that if we carry out a full relaxation of the structure of UO_2 using the present computational details without symmetry constraint, we obtain a tetragonal structure characterized by a shortening of the lattice constant c. This point is also often mentioned in the literature, [56,74] which is essentially due to the approximation of the magnetic interaction of the uranium valence electrons by a collinear $1k$ order antiferromagnetic instead of the non-collinear $3k$ one. The calculated bulk modulus B is comparable with the experimental results, even if it is observed that the LDA+U as well as the GGA+U calculations (Table 1) tend to overestimate and to underestimate it, respectively. We consider the LDA+U results most suitable to represent the bulk properties of UO_2 since

its deviation with respect to the experiments is the smallest (Table 1). Therefore, the difference in the unit-cell constant Δa (between the LDA+U calculation and the experimental results) does not represent a significant change in the U - O and U - U bond distances (see Table 1) in the bulk UO_2, which is a crucial prerequisite for the consideration of the molecular cluster $(UO_8)^{12-}$ embedded in UO_2 described in the next section.

The model of the optical properties due to the uranium $nd^{10}5f^2 \rightarrow nd^9 5f^3$ transitions, with n = 3, 4 and 5 is tackled here by means of multiplet energy levels calculation based on ligand field concept with two-open-shell configurations of d and f electrons. It is necessary to take a molecular cluster representing the U centre and its ligand environment instead of the full periodical model. This molecular cluster consists of one uranium centre plus eight oxygen ligands placed in the vertices of a regular cube (see Figure 1). The bond length between U and O is fixed to the LDA results given in Table 1. Moreover the long-range influence of the UO_2 lattice is reproduced by adding a series of point charges placed at the crystallographic positions of the U and O atoms in UO_2. [75] We have carried out DFT calculations using the ADF suite of programs. [29-31]

The first step comprises a DFT calculation considering the ground electron configuration of U^{4+}, *i.e.* $5f^2$. Since the Wyckoff position of the U site is octahedral, the $5f$ orbitals split by the ligand field interaction (eqn. 7) into three distinct energy levels forming the basis of the a_{2u} t_{1u} and t_{2u} irreducible representations of the O_h point group. The AOC set-up occupies each component of the $5f$ orbitals with a fractional electron occupation of 2/7. [21] In this situation, the density belongs to the totally symmetric irreducible representation of the O_h point group under which the ligand field Hamiltonian (eqn. 1) is invariant. The three-fold degenerate t_{1u} level has theoretically the lowest energy, whereas the a_{2u} is strongly destabilized partly due to the specific cubic arrangement of the eight O ligands.
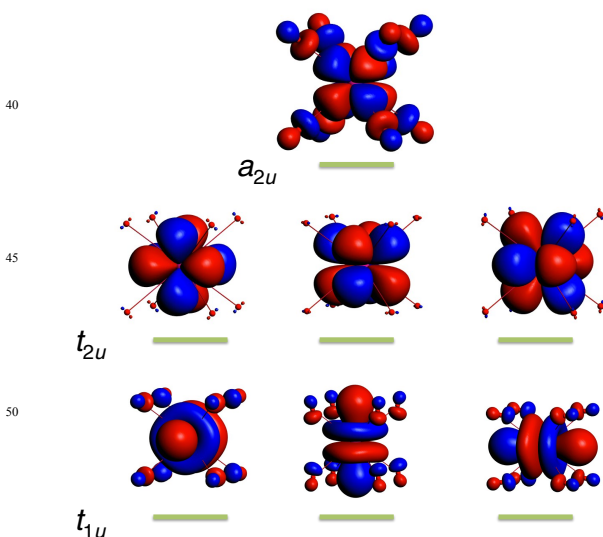
Fig. 2 Representation of the energy splitting of the $5f$ Kohn-Sham orbitals of U^{4+} in $(UO_8)^{12-}$ embedded in UO_2 obtained from the output of an AOC-type calculation, populating 2 electrons in the seven-fold $5f$ orbitals.

The splitting pattern of the $5f$ orbitals of U^{4+} in the cluster $(UO_8)^{12-}$ embedded in the bulk UO_2 is graphically represented in Figure 2 together with the molecular orbitals scheme as result of linear combination of atomic orbitals.

The second step consists of carrying out DFT calculations taking into account the core or semi-core electron excitations originating from the $3d$, $4d$ and $5d$ orbitals of U^{4+} to the partially filled $5f$ levels. We deal with the electron configurations $nd^9 5f^3$ with n = 3, 4 and 5, respectively. In these situations the AOC includes two-open-shell systems with d and f electrons, which populates 3/7 electrons in each component of the $5f$ orbitals (Figure 2), plus 9/5 electrons in each component of the $3d$ or $4d$ or $5d$ orbitals, respectively. [21] In the O_h point group, these d orbitals transform into the t_{2g} and e_g irreducible representations. We stress that the splitting of the $3d$, $4d$ and $5d$ orbitals, as obtained theoretically here, is relatively small and will be completely superseded by the effect of the spin-orbit coupling interaction.

To find the ligand field potential in the definition as given by eqn. 7, we use the eigenvalues of the Kohn-Sham orbitals with dominant $5f$ and nd (with n = 3, 4 and 5) character obtained from the AOC calculations. These Kohn-Sham orbital energies match with the quantities $<a_{2u}|H_{LF}|a_{2u}>$, $<t_{2u}|H_{LF}|t_{2u}>$, and $<t_{1u}|H_{LF}|t_{1u}>$ representing the eigenvalues of the $5f$ ligand field (eqn. 7), and $<t_{2g}|H_{LF}|t_{2g}>$ and $<e_g|H_{LF}|e_g>$ of the nd ligand field. Therefore, one can deduce the ligand field parameters $B^4_0(ff)$, $B^6_0(ff)$ and $B^4_0(dd)$ from DFT as follows:

$$B^4_0(ff) = -\frac{39}{44}\left(3\langle a_{2u}|H_{LF}|a_{2u}\rangle + 4\langle t_{2u}|H_{LF}|t_{2u}\rangle\right) \quad (8)$$

$$B^6_0(ff) = \frac{36}{11(2+\sqrt{2})}\left(\langle a_{2u}|H_{LF}|a_{2u}\rangle + 2\langle t_{1u}|H_{LF}|t_{1u}\rangle\right) \quad (9)$$

$$B^4_0(dd) = \frac{21}{10}\left(\langle e_g|H_{LF}|e_g\rangle - \langle t_{2g}|H_{LF}|t_{2g}\rangle\right) \quad (10)$$

One may note that H_{LF} (eqn. 7) is a traceless matrix (*i.e.* $B^0_0(ff) = 0$ and $B^0_0(dd) = 0$). Therefore, the orbital energies extracted from DFT were adjusted around the barycenter of the $5f$ orbitals, and also for the nd orbitals. The mixed term parameters due to the ligand field related to the $d - f$ interaction are by definition zero since the f and the d orbitals possess different parity in the O_h point group. [26]

The spin-orbit coupling constants ζ are obtained by means of the ZORA spin-orbit calculations. [21] For the $3d$, $4d$ and $5d$ electrons, ζ_{3d}, ζ_{4d} and ζ_{5d} are determined from the energy difference between the $d_{5/2}$ and $d_{3/2}$ components of the d orbitals: the ligand field interaction (eqn. 7) being negligible (see Table 2). For the $5f$ electrons, ζ_{5f} is obtained by mapping the DFT based ZORA spin-orbit results with the matrix elements of the spin-orbit coupling interaction (eqn. 6) plus the ligand field potential (eqn. 7). In previous works [76,77] we have presented the details of the mapping algorithm and involved procedures to estimate ζ, illustrating the influence of the ligands on the spin-orbit coupling in particular that the coupling constant may vary notably with the orbital energy. [76,78]. The $5f$ orbitals in O_h symmetry split into six spinors (spin-orbit terms), as the molecular orbitals t_{1u}, t_{2u} and a_{2u} (see Figure 2), respectively, transform to $g_{3/2u} + e_{1/2u}$, $e_{5/2u} + g_{3/2u}$ and $e_{5/2u}$, irreducible representations of the O_h^*

double group. Therefore, using symmetry analysis we have obtained a set of spin-orbit coupling constants. Thus, the calculated spin-orbit coupling constant of $5f$ electrons reported in Table 2 is an averaged value used for the ligand-field calculation.

The calculated ζ_{5f} value in Table 2 is in agreement with the spin-orbit coupling constant reported in ref. [79] that was derived for the linear UO_2 molecule (uranium $5f^2$ configuration) using CASPT2. [80] We also note that the parameter ζ_{5f} changes from 2- to 3-electron population of the uranium $5f$ orbitals (see Table 2), in agreement with previous studies based on four component relativistic calculations of americium in AmO_2^{3+}(with $5f^2$ configuration), AmO_2^{2+} ($5f^3$) and AmO_2^+ ($5f^4$) molecular systems. [79] The Slater-Condon integrals in eqn. 3, 4 and 5 are calculated by means of the radial functions of the Kohn-Sham orbitals with dominant $5f$ and $3d$, $4d$, and $5d$ character. A graphical representation of the radial functions of $5f$ Kohn-Sahm orbitals is shown in Figure 3. The corresponding results of nd orbitals are available in the ESI† (see Figure S2). According to eqn. 3, there are four independent parameters given by the four different k values: 0, 2, 4 and 6. However according to eqn. 4 and eqn. 5, there are three independent parameters discriminated by $k = 0, 2,$ 4 and $k = 1, 3, 5$, respectively for the F and the G integrals. In total, there are ten Slater-Condon integrals to be considered in the calculation of the $nd^{10}5f^2 \rightarrow nd^95f^3$ transitions, with n = 3, 4 and 5. We may consider four different situations, giving rise to the series of mentioned parameters tabulated in the four columns of Table 2.

Table 2 Calculated parameters (in eV) corresponding to the Slater-Condon integrals, the spin-orbit coupling constants and the ligand field potential of U^{4+} in the molecular cluster $(UO_8)^{12-}$ embedded in UO_2; obtained for the ground electron configuration $5f^2$ as well as the core and semi-core electron excitations $3d^95f^3$, $4d^95f^3$, $5d^95f^3$ configurations.

	$5f^2$	$3d^95f^3$	$4d^95f^3$	$5d^95f^3$
$F^0(ff)$	0	0	0	0
$F^2(ff)$	6.3133	6.0514	6.0340	6.0327
$F^4(ff)$	4.0717	3.9161	3.9058	3.9034
$F^6(ff)$	2.9737	2.8645	2.8575	2.8552
$F^0(df)$	-	517.47	107.55	14.39
$F^2(df)$	-	1.8605	3.6248	7.7046
$F^4(df)$	-	0.8706	1.4584	4.9201
$G^1(df)$	-	1.4691	0.6425	9.0266
$G^3(df)$	-	0.8870	0.6931	5.5682
$G^5(df)$	-	0.6201	0.5858	3.9703
ζ_{5f}	0.2257	0.2071	0.2098	0.2151
ζ_{3d}	-	71.7436	-	-
ζ_{4d}	-	-	16.8803	-
ζ_{5d}	-	-	-	3.2573
$B_0^4(ff)$	-1.7201	-1.3857	-1.4094	-1.5195
$B_0^6(ff)$	0.3962	0.3593	0.3666	0.3946
$B_0^4(dd)$	-	-0.0235	-0.0504	-0.0015
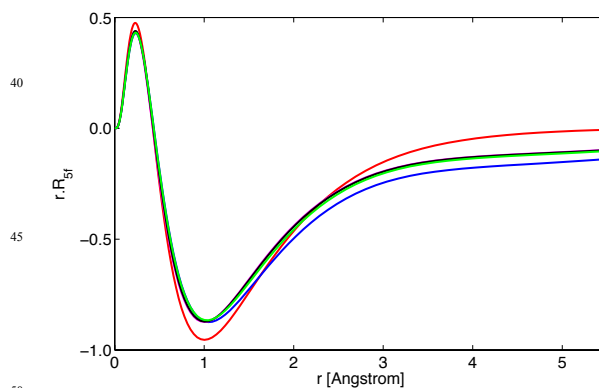
Fig. 3 Graphical representation of U^{4+} radial functions ($5f_{xyz}$ Kohn-Sham orbitals) in UO_2: electron configuration $5f^2$ (in blue), $3d^95f^3$ (in magenta), $4d^95f^3$ (in black) and $5d^95f^3$ (in green). The corresponding result for a free U^{4+} ion is also shown (in red).

In the ground state of the U^{4+} *i.e* the $5f^2$ electron configuration, the Slater-Condon parameters corresponding to the mixed $d - f$ terms are not important since we are in the presence of single-open-shell of f electrons. Accordingly, the spin-orbit coupling constant corresponding to the d shell is ignored as well as the parameter for the ligand field potential of the $d - d$ interaction. Then, we have the three situations where one electron is promoted from the $3d$, $4d$ or $5d$ shells to the $5f$. In all three cases, the mixed Slater-Condon parameters do not anymore vanish, as they are important to represent the interaction between the two-open-shell electron configurations. On the other hand, the Slater-Condon parameters representing the $f - f$ terms are not comparable with the parameters obtained for the ground configuration. They must be different because they take into account the presence of three electrons instead of the earlier two ones on the emulation of the radial function of the $5f$ Kohn-Sham orbitals. In the calculation of the multiplet energy levels, they will be present in the diagonal element of the ligand field Hamiltonian (eqn. 1) corresponding to the nd^95f^3 (with n = 3, 4, and 5) matrix interaction.

The phenomenological Hamiltonian in eqn. 1 can be represented by a block matrix of 3731 times 3731 elements. By definition, it is a complex and Hermitian matrix composed by a sub-block diagonal of 91 times 91 elements corresponding to the ground $5f^2$ configuration of U^{4+} and a sub-block diagonal of 3640 times 3640 elements proper to the d^95f^3 configuration. The sub-block of the $5f^2$ interactions is parameterized by only the ground state values in Table 2, whereas the sub-block of the $d - f$ interactions may take the different values in Table 2 according to n = 3, 4 and 5, respectively.

Considering the ground state configuration, in terms of Russell-Saunders coupling, two electrons in the $5f$ orbitals induce seven spectral terms with different energy levels. They are constituted by the high spin ^3P, ^3F and ^3H states as well as the low spin ^1S, ^1D, ^1G and ^1I states. The Hund's rules allow the determination of the ground state, in this case ^3H. By inclusion of the spin-orbit coupling interaction (eqn. 6), all the spin-triplet states split into energy levels discriminated by their J values namely, $^3P_0$, $^3P_1$, $^3P_2$, $^3F_2$, $^3F_3$, $^3F_4$, $^3H_4$, $^3H_5$ and $^3H_6$. Together with the earlier spin-

singlet states, it results in total thirteen states, in which the ground state becomes $^3H_4$ applying once more the Hund's rules. Finally the ligand field interaction, which accounts for the presence of the oxygen ligands, splits all the spectral terms in various ligand field levels. The present octahedral coordination allows in total forty energy levels.

The values of the parameters in Table 2 are comparable with the experimental findings, although it is observed that the DFT slightly overestimates some values. We can refer to the experimental results in ref. [81,82] corresponding to the spectroscopy of the free U^{4+} ion. The best reproduction of the energies of the thirteen spectral terms proper to the free ion is achieved using the parameters (in eV): $F^2(ff) = 6.44$, $F^4(ff) = 5.30$, $F^6(ff) = 3.44$ and $\zeta_{4f} = 0.24$. [82] These parameters will be reduced by the nephelauxetic effect [83] when the U^{4+} is being coordinated with ligands, for instance in the present UO_2 case. In this context we can refer to the magneto-optical experiments of UO_2 in ref. [84,85], where the following Slater-Condon and spin-orbit coupling parameters (in eV): $F^2(ff) = 5.34$, $F^4(ff) = 4.57$, $F^6(ff) = 3.64$ and $\zeta_{4f} = 0.22$ are deduced. The overestimation due to the DFT is mainly visible for $F^2(ff)$, which is also accompanied by an underestimation of $F^4(ff)$ and $F^6(ff)$. In ref. [86], the experimentally deduced ligand field parameters are -3.080 eV for $B^4_0(ff)$ with a fixed value for the ratio $B^4_0(ff)/B^6_0(ff)$. On the other hand, the inelastic neutron scattering experiment in [87] yields $B^4_0(ff) = -0.984$ eV and $B^6_0(ff) = 0.424$ eV. It is clear that the reproduction of the experimental $B^6_0(ff)$ parameter by DFT (Table 2) is realized, whereas $B^4_0(ff)$ is in the interval of two different experimental values. The calculated parameters corresponding to the $d^9 5f^3$ configurations (Table 2) are comparable to the values related to the d - f transitions obtained from Hartree-Fock calculations of U^{4+} in ref. [88]

The energies of the multiplet levels arising from the $5f^2$ configuration of U^{4+} in UO_2 using the cluster model $(UO_8)^{12-}$ are calculated and graphically represented in Figure 4.
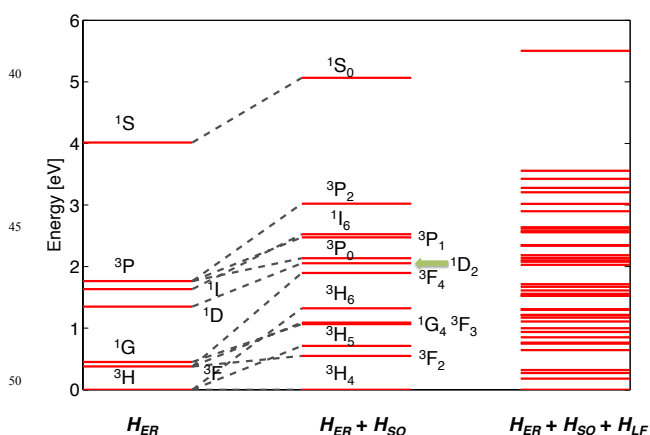
Fig. 4 Calculated multiplet energy levels (in red) arising from the ground $5f^2$ electron configuration of U^{4+} in UO_2 taking successively the effect of the inter-electron repulsion (left-hand-side), the inter-electron repulsion plus spin-orbit coupling (middle) and the inter-electron repulsion plus spin-orbit coupling plus ligand field interaction (right-hand-side) into account.

Table 3 Selected theoretical (Calc.) energy levels (in eV) arising from the ground $5f^2$ electron configuration of U^{4+} in the cluster $(UO_8)^{12-}$ embedded in UO_2, together with three reference data (Exp.) based on fit to the experiments.

$5f^2$ Levels	Calc.	Exp.		
		1[a]	2[b]	3[c]
T_2	0	0	0	0
E	0.1805	0.1501	0.170	0.230
T_1	0.2714	0.1667	0.624	0.525
A_1	0.3195	0.1748	0.710	0.630
T_1	0.6434	-	0.727	0.720
E	0.7484	-	0.918	0.850
T_2	0.7640	-	0.809	0.765
E	0.8518	-	1.183	1.110
T_2	0.9375	-	1.042	0.935
T_2	0.9979	-	1.210	1.160
T_1	1.1083	-	1.274	1.215
A_1	1.1708	-	1.110	1.035
T_1	1.2112	-	1.299	1.280
A_2	1.2153	-	1.296	-

[a] taken from ref. [87]; [b] taken from ref. [84]; [c] taken from ref. [89]

We present three series of energy levels in Figure 4 representing first the influence of the inter-electron repulsion H_{EE} (eqn. 2), secondly the influence of the sum of H_{EE} and the spin-orbit coupling interaction H_{SO} (eqn. 6) and finally the influence of the sum of H_{EE}, H_{SO} and the ligand field interaction H_{LF} (eqn. 7). This is important in order to show the evolution of the spectral terms energy with respect to the three components, which constitute the Hamiltonian in eqn. 1. The highest energy level obtained for the $5f^2$ corresponds to the single degenerate $^1S_0$ state with a calculated energy of 5.504 eV (Figure 4). For info, in the free-ion spectroscopy, this state is experimentally found to have an energy of 5.407 eV. [82] The spectral terms are identified and labelled for the H_{EE} multiplets as well as for the $H_{EE} + H_{SO}$ (Figure 4). However, the labelling of the spectral terms due to $H_{EE} + H_{SO} + H_{LF}$ is omitted for clarity in Figure 4. The forty states obtained at this stage form the basis of the following representations: A_1 (seven times), A_2 (three times), E (nine times), T_1 (nine times) and T_2 (twelve times). Selected energy levels corresponding to them are collected in Table 3 (see also the ESI† Table S1 for the whole manifold of the ligand field multiplet of the $5f^2$ configuration).

In Table 3, the calculated multiplet energy levels of the uranium $5f^2$ configuration in UO_2 are compared with some theoretical and experimental results available in the literature. The multiplet energy levels in second column of Table 3 have been computed by diagonalizing the ligand field Hamiltonian (eqn 1) with a ground state (lowest T_2 state) energy correction. Therefore, these energy levels represent the vertical excitation energies of the ground T_2 state, hence, can be compared with the corresponding excitation energies measured in the experiments. The measured energy values in the third column of Table 3 are associated with $T_2 \rightarrow E$, $T_2 \rightarrow T_1$, and $T_2 \rightarrow A_1$ transitions reported in ref. [87].

These energy values have been obtained by comparing the neutron energy gain or loss spectra (acquired in inelastic high-resolution neutron scattering experiments) with the detailed ligand field calculations. The fourth column in Table 3 shows the transition energies as determined using ligand field calculations, which also corroborate the magnetic susceptibility measurements in UO$_2$. [84] The last column in Table 3 lists the excitation energies obtained from optical absorption data measured by probing the intra $5f^2 \rightarrow 5f^2$ transitions and multiphonon excitations in UO$_2$. [89] Although the ligand field model has always been considered to interpret the experimental data in the studies highlighted above, it becomes also evident from Table 3 that all energy values are not throughout in good agreement with each other. In particular, we note that the energy values in ref. [84] and ref. [89] of T$_2$ → T$_1$ and T$_2$ → A$_1$ transitions differ significantly when compared to those presented in ref. 87. The exact reason of this discrepancy is unclear. We believe it is the result of methodological differences between studies under different experimental conditions. Moreover, the data in third to fifth columns of Table 3 are estimates of a model's parameters based on the evaluation of fits to experimental data with theoretical functions. Therefore, it seems more reasonable to consider the results of high-resolution neutron scattering experiment in the study by Amoretti and co-workers, [87] which would be best suited to validate our LFDFT results. The most important aspect is the splitting of the ground state of the free ion ($^3H_4$) in terms of ligand field energy, where by group theoretical consideration we obtain four levels. A$_1$, E, T$_1$ and T$_2$. The calculation designates the T$_2$ as the ground state (Table 3) in line with the above referenced works.

Considering the d^9f^3 electron configuration, we address the problem as the product of the multiplets of f^3 configuration with a d electron. This is equivalent to the product of f^3 with a d hole, *i.e.* d^9 in this work. The parent f^3 configuration leads to spectral terms with quartets and doublets spin multiplicity, [90] forming the basis of 364 single determinants. When we add the d electron (or equivalently the d hole), we obtain 158 spectral terms, which form the basis of 3640 single determinants. The resulting spectral terms of the d^9f^3 configuration are then: ^5S, ^5P (two times), ^5D (four times), ^5F (three times), ^5G (four times), ^5H (three times), ^5I (two times), ^5K, ^5L, ^3S (three times), ^3P (seven times), ^3D (eleven times), ^3F (twelve times), ^3G (thirteen times), ^3H (eleven times), ^3I (nine times), ^3K (six times), ^3L (four times), ^3M (two times), ^3N, ^1S (two times), ^1P (five times), ^1D (seven times), ^1F (nine times), ^1G (nine times), ^1H (eight times), ^1I (seven times), ^1K (five times), ^1L (three times), ^1M (two times) and ^1N.

The aforementioned spectral terms originate from the inter-electron repulsion represented by eqn. 2, but they are split by the spin-orbit coupling (eqn. 6) and the ligand field interaction (eqn. 7) in the same manner as the process already described for the $5f^2$ configuration (see Figure 4). We note that the consideration of the $3d^95f^3$ or $4d^95f^3$ or $5d^95f^3$ configurations does not change the definition of the spectral terms but affects the spectral energies *via* different parameterization of the Hamiltonian in eqn. 1. The variation of the Slater-Condon parameters $F^k(ff)$ in the series $3d^95f^3$, $4d^95f^3$ and $5d^95f^3$ configurations is not significant (Table 2). However the mixed terms Slater-Condon for $d - f$ interactions increases in the same series showing the relative interaction

between the core d shells and the valence $5f$. This interaction is relatively weak considering the $3d - 5f$ situation, whereas it comes globally important in the cases of the $4d - 5f$ and $5d - 5f$. Therefore, multiplet levels are the main contributors to the XANES spectra of UO$_2$ at the uranium M$_{4,5}$, N$_{4,5}$ and more importantly at the O$_{4,5}$ edges, their spectral features may not be reflected in the experimental spectrum.

The multiplet energy levels of the $3d^95f^3$, $4d^95f^3$, and $5d^95f^3$ configurations of U^{4+} in UO$_2$ are calculated by diagonalizing the ligand field Hamiltonian (eqn. 1) with a ground state energy correction corresponding to the lowest T$_2$ state of the $5f^2$ configuration (see Table 3). The results are graphically represented in Figure 5, Figure 6 and Figure 7, respectively (in the ESI† the numerical data corresponding to these energy levels are available in the Table S2, Table S3 and Table S4).
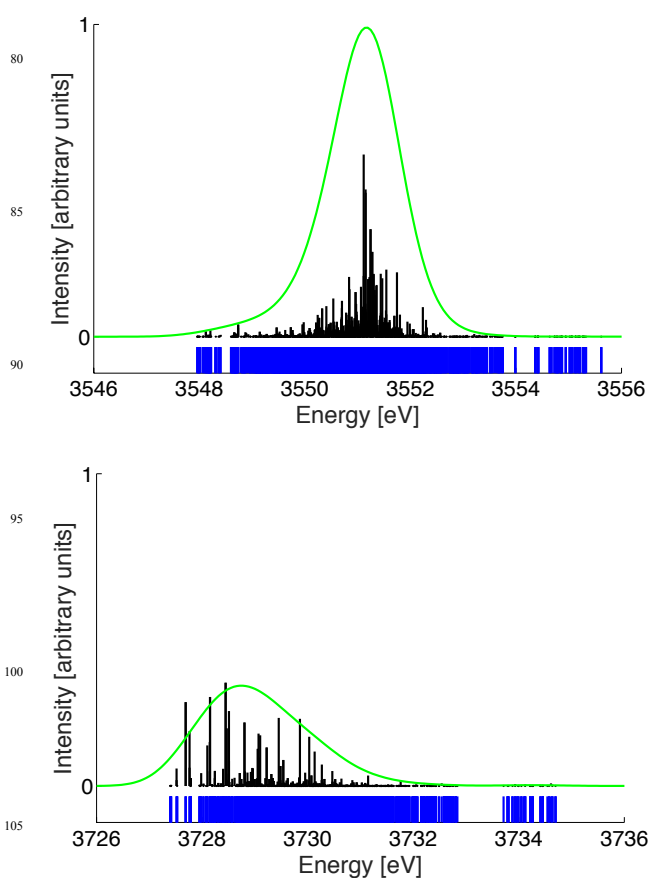
Fig. 5 Calculated multiplet energy levels (in blue colour) of the $3d^95f^3$ electron configuration of U^{4+} in UO$_2$ (see also the ESI† Table S2); together with the intensities of the absorption $3d^{10}5f^2$ (T$_2$) → $3d^95f^3$ transitions, *i.e.* oscillator strength (in black colour) representing the uranium M$_5$ and M$_4$ edges X-ray absorption spectrum of UO$_2$ in the energy intervals 3546 – 3556 eV (upper-panel) and 3726 – 3736 eV (lower-panel), respectively. The green curve represents oscillator strengths convoluted with Gaussian bands with a width of 0.5 eV.

The DFT calculations yield relatively larger values of ζ_{3d} and ζ_{4d} (see Table 2), as also has been underlined previously in the literature. [91] The d orbitals split into two distinct components: $d_{3/2}$ and $d_{5/2}$. This, in turn leads the multiplet energy levels separated into two blocks as illustrated in Figure 5 and Figure 6. The two blocks, which are shown in the upper-panel and lower-panel of the figures, represent the excitations of one electron from the $d_{5/2}$ and $d_{3/2}$ of U^{4+}, respectively. In Figure 7, the value of ζ_{5d} (see Table 2) is not large enough to induce the same earlier graphical representations insofar as all the multiplet levels are gathered in the same energy interval.

The core d level X-ray absorption mechanisms are in principle initiated by the $d^{10}f^2 + h\nu \rightarrow d^9f^3$ transitions, [92] which we have resumed here by the simpler notation: $d^{10}f^2 \rightarrow d^9f^3$. Because of the mixing between the d and f electrons, the $d^{10}f^2 \rightarrow d^9f^3$ transitions fulfil the electric dipole moment selection rule, giving rise to strong line intensities in the absorption spectra. It is also possible to include the electric-quadrupole transitions and/or the magnetic-dipole transitions in our calculations. But one may note that such transitions may result in very small intensities relative to the electric dipole allowed transitions in a measured X-ray absorption spectrum. [93,94] For UO_2, quadrupole transitions involve electron transfers $3d^{10}5f^2 \rightarrow 3d^95f^26s^1$ and $3d^{10}5f^2 \rightarrow 3d^95f^26d^1$ in three-open-shell configurations. In this work, our calculations are restricted to the systems with only two-open-shell of d and f electrons. In a future work, we plan to extend the LFDFT approach to include the calculations of electron configurations with more than two non-equivalents electrons (*i.e.* ligand field with three-open-shell systems). The multiplet energy levels arising from such multiple electron configurations will also be able to predict for instance possible shake-up satellites in the absorption spectra.

To model the line intensities, we use the matrix element of the electric dipole moment operator D (eqn. 11). D consists of the product between a radial integral, involving the radial functions R of Kohn-Sham orbitals of dominant f and d characters, and an angular integral, which can be associated with the Clebsh-Gordan coefficients. [94]

$$D_\mu = \frac{\sqrt{4\pi}}{3} \langle R_{nd} | r | R_{5f} \rangle \langle Y_{2,md} | Y_{l,\mu} | Y_{3,mf} \rangle \qquad (11)$$

D is important for the computation of the oscillator strengths related to the $d^{10}f^2 \rightarrow d^9f^3$ transitions, by distributing its elements over the whole manifold of the multi-electronic configuration interactions obtained from the ligand field Hamiltonian (eqn. 1). The oscillator strengths are calculated taking as initial state the three-fold degenerate T_2 level originated from the $^3H_4$ state (Figure 4) representative of the ground $5f^2$ configuration of U^{4+} (see Table 3). Furthermore, we consider the whole manifold of the d^9f^3 multiplets as final states. The oscillator strengths are also graphically represented using bar diagrams placed above the multiplet energy levels for the $3d^{10}5f^2$ (T_2) $\rightarrow 3d^95f^3$, $4d^{10}5f^2$ (T_2) $\rightarrow 4d^95f^3$ and $5d^{10}5f^2$ (T_2) $\rightarrow 5d^95f^3$ transitions, respectively, in Figure 5, Figure 6 and Figure 7.

In these figures, the intensity plots along the ordinate are shown in arbitrary units, which are also normalized to unity either for the oscillator strengths or for the Gaussian convolution. The choice of the Gaussian convolution is motivated by the fact that we shall not intend to perform a full simulation of the X-ray absorption profile. Indeed such a simulation will require a special treatment of the broadening effect of the oscillator strengths, [95,96,97] which depends on different factors, which are not always tractable by pure first principles method. Thus the simulation of the spectral profile consists of pure Gaussian broadening of the oscillator strengths of all the multiplets in which they receive identical energy half-width of 0.5 eV. This energy width is in principle comparable with the energy resolution of synchrotron-based X-ray absorption spectroscopy experiments, depending on the proper selection of monochromator crystals [98,99] and detector systems. In the ESI†, evaluation of the Gaussian broadening effect of the oscillator strengths, taking different values for the half-width parameter can be found for the problem of $3d^{10}5f^2$ (T_2) $\rightarrow 3d^95f^3$, $4d^{10}5f^2$ (T_2) $\rightarrow 4d^95f^3$ and $5d^{10}5f^2$ (T_2) $\rightarrow 5d^95f^3$ transitions, respectively, in Figure S3, Figure S4 and Figure S5.
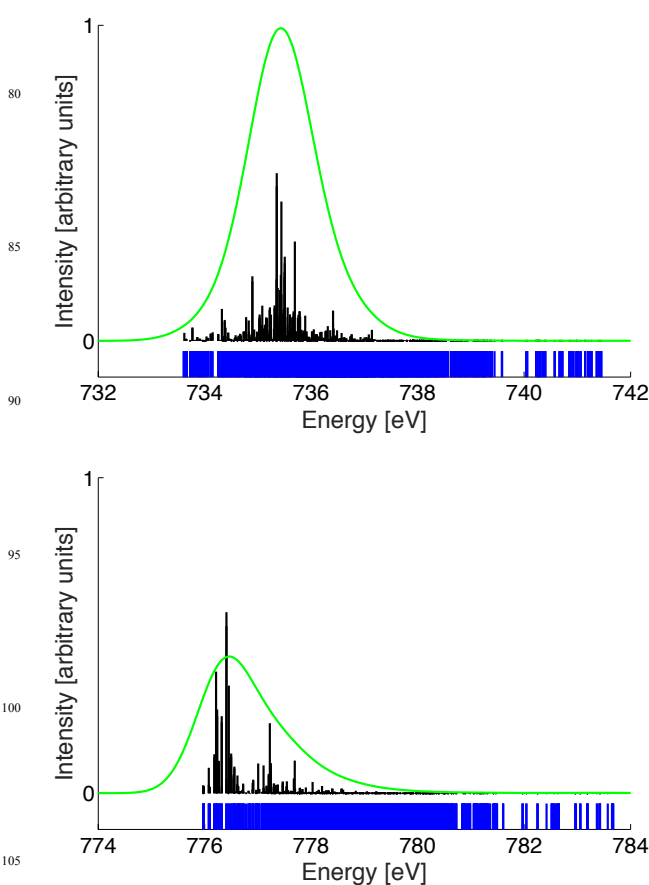
Fig. 6 Calculated multiplet energy levels (in blue colour) of the $4d^95f^3$ electron configuration of U^{4+} in UO_2 (see also the ESI† Table S3); together with the intensities of the absorption $4d^{10}5f^2$ (T_2) $\rightarrow 4d^95f^3$ transitions, *i.e.* oscillator strength (in black colour) representing the uranium N_5 and N_4 edges X-ray absorption spectrum of UO_2 in the energy intervals 732 – 742 eV (upper-panel) and 774 – 784 eV (lower-panel), respectively. The green curve represents the oscillator strengths convoluted with Gaussian bands with a width of 0.5 eV.

Figure 5 shows the multiplet energy levels of the $3d^9 5f^3$ configuration of U^{4+} in UO_2 together with the calculated X-ray absorption spectrum of the uranium $3d$ edge. The spectrum is dominated by the spin-orbit coupling interaction of the $3d$
5 electrons. Therefore, it is characterized by the two intense absorptions, which maxima are located in the energy scale at 3551 eV and 3729 eV. These absorptions correspond to the M_5 and M_4 spectra, respectively found in the upper-panel and lower-panel of Figure 5. The M_4 spectrum is less intense than the M_5
10 one; the ratio between their intensities (*i.e.* the sum over the oscillator strengths belonging to each of them) represents 2.19. Besides, the oscillator strengths are mainly situated in the low and middle-range of the multiplet energy scale of the M_4 (Figure 5, lower-panel) and M_5 (Figure 5, upper-panel) spectra, whereas
15 in the high-energy range the transitions are strictly forbidden. They fulfil the dipole moment selection rule since the main contributor of the intensity is attributed to the ligand field components of the $3d^9 5f^3$ multiplets having *J* values of 3, 4 and 5. In ref. [100] the XANES spectra for UO_2 at the uranium M_4 and
20 M_5 edges measured by total-electron-yield-techniques is reported. Although both experimental XANES spectra do not exhibit visible multiplet structure, [100] intense white-lines are observed due to the $3d$ - $5f$ optical transitions. They are accompanied by small satellites, which were discussed in terms of multiple
25 scattering resonances containing information on the local structure around the absorbing uranium ion. [100]

Figure 6 shows the multiplet energy levels of the $4d^9 5f^3$ configuration of U^{4+} in UO_2 together with the calculated absorption spectrum of the uranium $4d$ edge. We still retrieve the
30 same characteristic as the earlier Figure 5 since the spectrum is also dominated by the spin-orbit coupling of the $4d$ electrons. Two intense absorptions are determined, which maxima are located in the energy scale at 735.3 eV and 776.5 eV. These absorptions represent the N_5 and N_4 spectra, respectively, shown
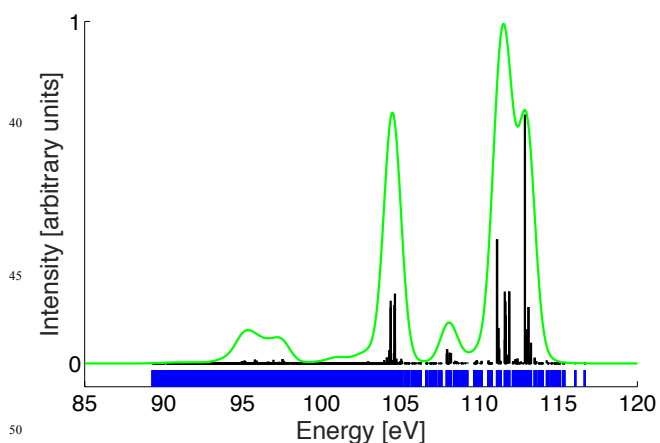35 in the upper-panel and lower-panel of Figure 6.

Fig. 7 Calculated multiplet energy levels (in blue colour) of the $5d^9 5f^3$ electron configuration of U^{4+} in UO_2 (see also the ESI† Table S4); together with the intensities of the absorption $5d^{10} 5f^2$
55 (T_2) → $5d^9 5f^3$ transitions, *i.e.* oscillator strength (in black colour) representing the uranium $O_{4,5}$ edge X-ray absorption spectrum of UO_2. The green curve represents the oscillator strengths convoluted with Gaussian bands with a width of 0.5 eV.

Figure 7 shows the multiplet energy levels of the $5d^9 5f^3$
60 configuration of U^{4+} in UO_2 together with the calculated absorption spectrum of the uranium $5d$ edge. The theoretical shape of the spectrum of the $O_{4,5}$ edge reveals the presence of several peaks, where three of them are noticeable (see also the ESI† Figure S5). They are situated in the energy scale at 96.0 eV,
65 104.6 eV and 112.5 eV. The highest energy peak possesses the most intense absorption (Figure 7). The influence of the spin-orbit coupling interaction of the $5d$ electrons is weak and the spectrum is mainly governed by the electrostatic inter-electron d – f repulsion. This is furthermore illustrated in Figure S6
70 provided in the ESI†. The three separate components of the total ligand field Hamiltonian (Eq. 1) are superimposed and summed to produce the total oscillator strength for the $5d^{10} 5f^2$ (T_2) → $5d^9 5f^3$ transitions. The described results demonstrate a dominant role of the inter-electron repulsion (H_{ER}) in determining the $O_{4,5}$
75 edge XANES of UO_2 (see the ESI† Figure S6).Therefore it is impossible to ascribe with energy ranges the O_5 and O_4 edges in the absorption spectrum. The lowest intense peak is strongly dependent on the spin-orbit coupling constant for $5d$ electrons. In ref. [101], X-ray absorption spectroscopy and electron energy-
80 loss spectroscopy have been employed to probe the electronic transitions from the $5d$ semi-core level of uranium in UO_2. It is observed that the $O_{4,5}$ absorption edges of UO_2 consist of three intense peaks, in line with our theoretical findings. Although we notice a slight shift in the energy scale (~2 eV) from the DFT
85 analysis, an overall agreement between computational and experimental results [101] is very encouraging.

The LFDFT results of UO_2 presented in this paper addressing the two-open-shell ligand field concept complement our recent work on the lanthanide systems, [19-22,26,27] shed light on the
90 understanding of the relationship between electronic states and XANES spectrum of actinide bearing compounds, and set the foundation for further work. A detailed study of uranium $L_{2,3}$ edges XANES spectra, [102,103] which would require a three-open-shell ligand field concept involving *p*, *f* and *d* orbitals (*i.e.*
95 the $2p^6 5f^2$ → $2p^5 5f^2 6d^1$ transitions), will be the subject of a forthcoming report with the aim of gaining deeper insights into the structural as well as electronic properties of irradiated UO_2 fuels. [104,105]

Conclusions

100 The demand for a theoretical description of the chemical, physical and crystallographic properties of uranium dioxide (UO_2) emerges from the fact that UO_2 is an actinide-isotope containing material for nuclear fuel applications. Besides, the electronic structure of UO_2 attracts scientific attention because of
105 many quantum effects, associated with the *f* electrons in the conduction process, which are often not fully understood. The purpose of this work, yet independent of any experimental verification, is to simulate the uranium $M_{4,5}$, $N_{4,5}$ and $O_{4,5}$ edges XANES of UO_2 exploiting the power of the LFDFT approach for
110 electronic structure calculations in relation with the X-ray absorption mechanisms at separate (low to high) energy regime. XANES is a fingerprint of the electronic structure, more specifically of the valence state of the absorbing atoms.

To achieve a quantitative understanding of this development and
115 appraisal of the corresponding XANES profiles, we have drawn

some points on the description of the core and semi-core *d* electron excitation process through its interaction with the valence electrons of U^{4+} in UO_2. The relevant model, which we use to solve the electronic structure problem, is based on the LFDFT algorithm. The LFDFT is a computational code merging the power of non-empirical DFT-based calculations with a phenomenological model. With this theoretical modelling, we have obtained parameters corresponding to the Slater-Condon integrals, the spin-orbit coupling interaction and the ligand field potential, which allowed computation of the multiplet energy levels arising from the ground $5f^2$ and the excited $nd^9 5f^3$ electron configurations of U^{4+} in UO_2 with n = 3, 4 and 5. We have additionally calculated the oscillator strength due to the dipole allowed $nd^{10}5f^2 \rightarrow nd^9 5f^3$ transitions and corresponding XANES profiles of UO_2 at the uranium $M_{4,5}$, $N_{4,5}$ and $O_{4,5}$ edges. Our calculated absorption bands are in good agreement with experimental spectra. Calculations for the uranium $L_{2,3}$ edges is underway.

Acknowledgments

Notes and references

ᵃPaul Scherrer Institute, CH 5232 Villigen PSI, Switzerland
ᵇDepartment of chemistry of the University of Fribourg, Chemin du musée 9, CH 1700 Fribourg, Switzerland
Corresponding authors: harry.ra@hotmail.com; goutam.kuri@psi.ch

†Electronic supplementary information (ESI) available: Graphical representation of the total electronic energy versus the lattice constant volume of bulk UO_2 obtained at the LDA+*U* and GGA+*U* DFT levels of theory; Radial functions of the *3d*, *4d* and *5d* orbitals of U^{4+} in UO_2 within the $nd^9 5f^3$ elctron configurations; Numerical data of the multiplet energy levels corresponding to the ground state $5f^2$ configuration of U^{4+} in UO_2; Studies of the broadening effect of the calculated oscillator strengths seen in Figure 5, Figure 6 and Figure 7; Graphical representation of the infleucence of the three terms of the ligand field Hamiltonian (eqn.1) on the results of the $5d^{10}5f^2$ (T_2) $\rightarrow 5d^9 5f^3$ transitions; Numerical data for the multiplet energy levels of the $nd^9 5f^3$ configuration of U^{4+} in UO_2, with n = 3, 4 and 5 given in Figure 5, Figure 6 and Figure 7, respectively. See DOI: 10.1039/b000000x.

1   M. Dolg, Computational Methods in Lanthanide and Actinide Chemistry, John Wiley & Sons, United Kingdom, 2015.

2   J.-P. Dognon, *Coord. Chem. Rev.*, 2014, **266-267**, 110.

3   M. L. Neidig, D. L. Clark and R. L. Martin, *Coord. Chem. Rev.*, 2013, **257**, 394.

4   L. S. Natrajan, *Coord. Chem. Rev.*, 2012, **256**, 1583.

5   L. R. Morss, N. M. Edelstein and J. Fuger, The Chemistry of the Actinide and Transactinide Elements, 4th edition, Springer, The Netherlands, 2011.

6   K. T. Moore and G. van der Laan, *Rev. Modern Phys.*, 2009, **81**, 235.

7   M. A. Denecke, *Coord. Chem. Rev.*, 2006, **250**, 730.

8   H. Nitsche, *J. Alloys Compounds*, 1995, **223**, 274.

9   W. T. Cannall, G. L. Goodman, C. W. Williams, S. Lam and G. M. Jursich, *J. Less Common Metals*, 1989, **148**, 201.

10   O. Gunnarsson, D. D. Sarma and F. U. Hillebrecht, *J. Appl. Phys.*, 1986, **63**, 3676.

11   P. Thunström, I. Di Marco, A. Grechnev, S. Lebègue, M. I. Katsnelson, A. Svane and O. Eriksson, *Phys. Rev. B*, 2009, **79**, 165104.

12   B. W. Veal, D. J. Lam., H. Diamond and H. R. Hoekstra, *Phys. Rev. B*, 1977, **15**, 2929.

13   B. N. Figgis and M. A. Hitchman, Ligand Field Theory and Its Applications, Wiley-VCH, New York, 2000.

14   H. Bethe, *Ann. Phys.*, 1929, **295**, 133.

15   J. H. van Vleck, *J. Chem. Phys.*, 1935, **3**, 807.

16   C. Daul, *Int. J. Quantum Chem.*, 1994, **52**, 867.

17   M. Atanasov and C. Daul, *CHIMIA Int. J. Chem.*, 2005, **59**, 504.

18   M. Atanasov, C. A. Daul and C. Rauzy, *Struct. Bonding*, 2004, **106**, 97.

19   H. Ramanantoanina, W. Urland, F. Cimpoesu and C. Daul, *Phys. Chem. Chem. Phys.*, 2013, **15**, 13902.

20   H. Ramanantoanina, W. Urland, B. Herden, F. Cimpoesu and C. Daul, *Phys. Chem. Chem. Phys.*, 2015, **17**, 9116.

21   H. Ramanantoanina, M. Sahnoun, A. Barbiero, M. Ferbienteanu and F. Cimpoesu, *Phys. Chem. Chem. Phys.*, 2015, **17**, 18547.

22   H. Ramanantoanina, F. Cimpoesu, C. Göttel, M. Sahnoun, B. Herden, M. Suta, C. Wickleder, W. Urland and C. Daul, *Inorg. Chem.*, 2015, **54**, 8319.

23   B. R. T. Frost, Nuclear Fuel Elements: Design, Fabrication and Performance, Pergamonn Press, New York, 1982.

24   G. Kessler, *Progress in Nuclear Energy*, 2002, **40**, 309.

25   C. Degueldre, J. Bertsch, G. Kuri and M. Martin, *Energy Environ. Sci.*, 2011, **4**, 1651.

26   H. Ramanantoanina, W. Urland, F. Cimpoesu and C. Daul, *Phys. Chem. Chem. Phys.*, 2014, **16**, 12282.

27   H. Ramanantoanina, W. Urland, A. Garcia-Fuente, F. Cimpoesu and C. Daul, *Phys. Chem. Chem. Phys.*, 2014, **16**, 14625.

28   S. Hüfner, Optical spectra of transparent rare earth compounds, Academic Press, New York, 1978.

29   G. te Velde, F. M. Bickelhaupt, S. J. A. van Gisbergen, C. F. Guerra, E. J. Baerends, J. G. Snijders and T. Ziegler, *J. Comput. Chem.*, 2001, **22**, 931.

30   C. F. Guerra, J. G. Snijders, G. te Velde and E. J. Baerends, *Theor. Chem. Acc.*, 1998, **99**, 391.

31   E. J. Baerends, T. Ziegler, J. Autschbach, D. Bashford, A. Berces, F. M. Bickelhaupt, C. Bo, P. M. Boerrigter, L. Cavallo, D. P. Chong, L. Deng, R. M. Dickson, D. E. Ellis, M. van Faassen, L. Fan, T. H. Fischer, C. F. Guerra, A. Ghysels, A. Giammona, S. J. A. van Gisbergen, A. W. Götz, J. A. Groeneveld, O. V. Gritsenko, M. Gru¨ning, S. Gusarov, F. E. Harris, P. van den Hoek, C. R. Jacob, H. Jacobsen, L. Jensen, J. W. Kaminski, G. van Kessel, F. Koostra, A. Kovalenko, M. V. Krykunov, E. van Lenthe, D. A. McCormack, A. Michalak, M. Mitoraj, J. Neugebauer, V. P. Nicu, L. Noodleman, V. P. Osinga, S. Patchkovskii, P. H. T. Philipsen, D. Post, C. C. Pye, W. Ravenek, J. I. Rodriguez, P. Ros, P. R. T. Shipper, G. Schreckenbach, J. S. Seldenthuis, M. Seth, J. G. Snijders, M. Sola, M. Swart, D. Swerhone, G. te Velde, P. Vernooijs, L. Versluis, L. Visscher, O. Visser, F. Wang, T. Wesolowski, E. M. van Wezenbeek, G. Wiesenekker, S. K. Wolff, T. K. Woo and A. L. Yarkolev, ADF2014.01, available at http://www.scm.com.

32   P. J. Stephens, F. J. Devlin, C. F. Chabalowski and M. J. Frisch, *J. Phys. Chem.*, 1994, **98**, 11623.

33   H. Chermette, G. Hollinger and P. Pertosa, *Chem. Phys. Lett.*, 1982, **86**, 170.

34   E. van Lenthe, E. J. Baerends and J. G. Sniders, *J. Chem. Phys.*, 1994, **101**, 9783.

35   V. Vetere, P. Maldivi and C. Adamo, *J. Comput. Chem.*, 2003, **24**, 850.

36   L. Visscher and E. van Lenthe, *Chem. Phys. Lett.*, 1999, **306**, 357.

37   G. Kresse and J. Hafner, *Phys. Rev. B: Condens. Matter Mater. Phys.*, 1993, **47**, 558.

38   G. Kreese and J. Furthmüller, *Phys. Rev. B: Condens. Matter Mater. Phys.*, 1996, **54**, 11169.

39   S. H. Vosko, L. Wilk and M. Nusair, *Can. J. Phys.*, 1980, **54**, 1200.

40   J. P. Perdew, K. Burke and M. Ernzerhof, *Phys. Rev. Lett.*, 1996, **77**, 3865.

41   P. E. Blöchl, *Phys. Rev. B: Condens. Matter Mater. Phys.*, 1994, **50**, 17953.

42   G. Kresse and D. Joubert, *Phys. Rev. B: Condens. Matter Mater. Phys.*, 1999, **59**, 1758.

43 H. J. Monkhorst and J. D. Pack, *Phys. Rev. B: Condens. Matter Mater. Phys.*, 1976, **13**, 5188.

44 J. G. Tobin, S.-W. Yu, C. H. Booth, T. Tyliszczak, D. K. Shuh, G. van der Laan, D. Sokaras, D. Nordlund, T.-C. Weng and P. S. Bagus, *Phys. Rev. B: Condens. Matter Mater. Phys.*, 2015, **92**, 035111.

45 J. H. de Boer and E. J. W. Verwey, *Proceedings of the Physical Society*, 1937, **49**, 59.

46 N. F. Mott and R. Peierls, *Proceedings of the Physical Society*, 1937, **49**, 72.

47 J. Schoenes, *Physics Reports*, 1980, **63**, 301.

48 B. C. Frazer, G. Shirane, D. E. Cox and C. E. Olsen, *Phys. Rev.*, 1965, **140**, 1448.

49 L. E. Roy, T. Durakiewicz, R. L. Martin, J. E. Peralta, G. E. Scuseria, C. G. Olson, J. J. Joyce and E. Guziewicz, *J. Comput. Chem.*, 2008, **29**, 2288.

50 Y. Baer and J. Schoenes, *Solid State Commun.*, 1980, **33**, 885.

51 F. Jollet, T. Petit, S. Gota, N. Thromat, M. Gautier-Soyer and A. Pasture, *J. Phys.: Condens. Matter*, 1997, **9**, 9393.

52 S. W. Yu, J. G. Tobin, J. C. Crowhurst, S. Sharma, J. K. Dewhurst, P. Olalde Velasco, W. L. Yang and W. J. Siekhaus, *Phys. Rev. B: Condens. Matter Mater. Phys.*, 2010, **83**, 165102.

53 S. L. Dudarev, G. A. Botton, S. Y. Savrasov, C. J. Humphreys and A. P. Sutton, *Phys. Rev. B: Condens. Matter Mater. Phys.*, 1998, **57**, 1505.

54 R. Laskowski, G. K. H. Madsen, P. Blaha and K. Schwarz, *Phys. Rev. B: Condens. Matter Mater. Phys.*, 2004, **69**, 140408.

55 K. N. Kudin, G. E. Scuseria and R. L. Martin, *Phys. Rev. Lett.*, 2002, **89**, 26.

56 B. Dorado, B. Amadon, M. Freyss and M. Bertolus, *Phys. Rev. B: Condens. Matter Mater. Phys.*, 2009, **79**, 235125.

57 S. L. Dudarev, M. R. Castell, G. A. Botton, S. Y. Savrasov, V. Muggelberg, G. A. D. Briggs, A. P. Sutton and D. T. Goddard, *Micron*, 2000, **31**, 363.

58 D. Gryaznov, E. Heifets and D. Sedmidubsky, *Phys. Chem. Chem. Phys.*, 2010, **12**, 12273.

59 F. Gupta, G. Brillant and A. Pasturel, *Philosophical Magazine*, 2007, **87**, 2561.

60 F. Zhou and V. Ozolins, *Phys. Rev. B: Condens. Matter Mater. Phys.*, 2011, **83**, 085106.

61 B.-T. Wang, P. Zhang, R. Lizarraga, I. Di Marco and O. Eriksson, *Phys. Rev. B: Condens. Matter Mater. Phys.*, 2013, **88**, 104107.

62 A. Kotani and T. Yamazaki, *Progress of Theoretical Physics Supplement*, 1992, **108**, 117.

63 F. Grønvold, *J. Inorg. Nuc. Chem.*, 1955, **1**, 357.

64 C. Mieszczynski, G. Kuri, C. Degueldre, M. Martin, J. Bertsch, C. N. Borca, D. Grolimund, C. Delafoy and E. Simoni, *J. Nuc. Mater.*, 2014, **444**, 274.

65 H. A. Jahn and E. Teller, *Proc. R. Soc. London Ser. A*, 1937, **161**, 220.

66 I. B. Bersuker, *The Jahn-Teller Effect*, Cambridge University Press, Cambridge 2006.

67 J. J. Faber and G. H. Lander, *Phys. Rev. B: Condens. Matter Mater. Phys.*, 1975, **35**, 1770.

68 J. J. Faber and G. H. Lander, *Phys. Rev. B: Condens. Matter Mater. Phys.*, 1976, **14**, 151.

69 R. Caciuffo, G. Amoretti, P. Santini, G. H. Lander, J. Kulda and P. de V. Du Plessis, *Phys. Rev. B: Condens. Matter Mater. Phys.*, 1999, **59**, 13892.

70 G. Amoretti, R. Caciuffo, P. Santini, G. H. Lander, J. Kulda and P. de V. Du Plessis, *J. Appl. Phys.*, 1999, **85**, 4524.

71 F. D. Murnaghan, *Proc. Nat. Aca. Sci.*, 1944, **30**, 244.

72 F. Birch, *Phys. Rev.*, 1947, **71**, 809.

73 P. Nerikar, T. Watanabe, J. S. Tulenko, S. R. Philipot and S. B. Sinnott, *J. Nuc. Mater.*, 2009, **384**, 61.

74 B. Dorado, G. Jomard, M. Freyss and M. Bertolus, *Phys. Rev. B: Condens. Matter Mater. Phys.*, 2010, **82**, 035114.

75 The molecular cluster $(UO_8)^{12-}$ is surrounded by 122 point charges corresponding to 80 oxygen ions with $Q = -2$ and 42 uranium ions with $Q = +4$, which allow simulation of the Madelung potential representing the long range interaction due to the periodicity of the UO_2 crystal structure.

76 M. Atanasov, C. Rauzy, P. Baettig and C. Daul, *Int. J. Quantum Chem.*, 2005, **102**, 119.

77 C. Daul, E. J. Baerends and P. Vernooijs, *Inorg. Chem.*, 1994, **33**, 3538.

78 A. Goursot and H. Chermette, *Chem. Phys.*, 1982, **69**, 329.

79 F.-P. Notter, S. Dubillard and H. Bolvin, *J. Chem. Phys.*, 2008, **128**, 164315.

80 L. Gagliardi, M. C. Heaven, J. W. Krogh and B. O. Roos, *J. Am. Chem. Soc.*, 2005, **127**, 86.

81 J. F. Wyart, V. Kaufman and J. Sugar, *Physica Scripta*, 1980, **22**, 389.

82 C. H. H. van Deurzen, K. Rajnak and J. G. Conway, *J. Opt. Soc. Am. B*, 1984, **1**, 45.

83 C. K. Jørgensen, *Absorption Spectra and Chemical Bonding in Complexes*, Pergamon Press, Oxford 1962.

84 the parameters in [H. U. Rahman and W. A. Runciman, *J. Phys. Chem. Solids*, 1966, **27**, 1833] represent the reduced Slater-Condon integrals, which are translated here using the factors in [R. D. Cowan, *The theory of atomic structure and spectra*, University of California Press, Berkeley 1981].

85 A. Narita, *Int. J. Soc. Mat. Eng. Resources*, 1999, **7**, 106.

86 the parameters in [S. Kern, C.-K. Loong and G. H. Lander, *Phys. Rev. B: Condens. Matter Mater. Phys.*, 1985, **32**, 3051] are written within the Stevens notation, which are translated to Wybourne using the factors in [D. J. Newman and B. K. C. Ng, *Crystal Field Handbook*, Cambridge University Press, Cambridge 2000].

87 the parameters in [G. Amoretti, A. Blaise, R. Caciuffo, J. M. Fournier, M. T. Hutchings, R. Osborn and A. D. Taylor, *Phys. Rev. B: Condens. Matter Mater. Phys.*, 1989, **40**, 1856] are written within the Stevens notation, which are translated to Wybourne using the factors in [D. J. Newman and B. K. C. Ng, *Crystal Field Handbook*, Cambridge University Press, Cambridge 2000].

88 R. Caciuffo, G. van der Laan, L. Simonelli, T. Vitova, C. Mazzoli, M. A. Denecke and G. H. Lander, *Phys. Rev. B: Condens. Matter Mater. Phys.*, 2010, **81**, 195104.

89 J. Schoenes, *Journal de Physique Colloques*, 1980, **41**, C5-31.

90 C. W. Nielson and G. F. Koster, *Spectroscopic Coefficients for the p^n, d^n and f^n*, MIT Press, Boston 1963.

91 A. Goursot, E. Penigault and H. Chermette, *Chem. Phys. Lett.*, 1983, **97**, 215

92 L. E. Cox, W. P. Ellis and R. D. Cowan, *Phys. Rev. B: Condens. Matter Mater. Phys.*, 1985, **31**, 2467.

93 S. Debeer George, T. Petrenko and F. Neese, *J. Phys. Chem. A*, 2008, **112**, 12936.

94 J. S. Griffith, The Theory of Transition Metal Ions, Cambridge University Press, Cambridge, 1961.

95 M. O. Krause and J. H. Olivier, *J. Phys. Chem. Ref. Data*, 1979, **8**, 329.

96 F. M. F. de Groot, J. C. Fuggle, B. T. Thole and G. A. Sawatzky, *Phys. Rev. B: Condens. Matter Mater. Phys.,* 1990, **41**, 928.

97 K. Ogasawara, T. Iwata, Y. Koyama, T. Ishii, I. Tanaka and H. A dachi, *Phys. Rev. B: Condens. Matter Mater. Phys.*, 2001, **64**, 115413.

98 P. Oberta, U. Flechsig, M. Muntwiler and C. Quitmann, *Nuclear Instruments and Methods in Physics Research A*, 2011, **635**, 116.

99 F. Schaefers, M. Mertin and M. Gorgoi, *Review of Scientific Instruments*, 2007, **78**, 123102.

100 G. Kalkowski, G. Kaindl, W. D. Brewer and W. Krone, *Phys. Rev. B: Condens. Matter Mater. Phys.*, 1987, **35**, 2667.

101 K. T. Moore and G. van der Laan, *Ultramicroscopy*, 2007, **107**, 1201.

102 C. J. Nelin, P. S. Bagus and E. S. Ilton, *RSC Adv.*, 2014, **4**, 7148

103 C. South, A. Shee, D. Mukherjee, A. K. Wilson and T. Saue, Phys. Chem. Phys., 2016, DOI: 10.1039/c6cp00262e

104 C. Degueldre, M. Martin, G. Kuri, D. Grolimund and C. Borca, *J. Nuc. Mater.*, 2011, **416**, 142.

105 C. Mieszczynski, G. Kuri, J. Bertsch, M. Martin, C. N. Borca, C. Delafoy and E. Simoni, *J. Phys.: Condens. Matter.*, 2014, **26**, 355009

Physical Chemistry Chemical Physics Accepted Manuscript